SNR enhancement through phase dependent signal reconstruction algorithms for phase separated interferometric signals

Emily J. McDowell[1], Marinko V. Sarunic[2], Zahid Yaqoob[3], and Changhuei Yang[1,3]

[1]*Department of Bioengineering (MC 138-78), California Institute of Technology, Pasadena, CA, 91125*
[2]*School of Engineering Science, Simon Fraser University, Burnaby, B.C. Canada, V5A1S6*
[3]*Department of Electrical Engineering (MC 136-93), California Institute of Technology, Pasadena, CA, 91125*
emilymcd@caltech.edu

Abstract: We report several signal reconstruction algorithms for processing phase separated homodyne interferometric signals. Methods that take advantage of the phase of the signal are experimentally shown to achieve a signal-to-noise ratio (SNR) improvement of up to 5 dB over commonly used algorithms. To begin, we present a derivation of the SNR resulting from five image reconstruction algorithms in the context of a 3x3 fiber-coupler based homodyne optical coherence tomography (OCT) system, and clearly show the improvement in SNR associated with phase-based algorithms. Finally, we experimentally verify this improvement and demonstrate the enhancement in contrast and improved image quality afforded by these algorithms through homodyne OCT imaging of a *Xenopus laevis* tadpole. These algorithms can be generally applied in signal extraction processing where multiple phase separated measurements are available.

OCIS codes: (120.3180) Interferometry; (170.4500) Optical coherence tomography; (110.4280) Noise in imaging systems; (170.3880) Medical and biological imaging;

References and links

1. G. Lai and T. Yatagai, "Generalized phase-shifting interferometry," J. Opt. Soc. Am. A **8,** 822-827 (1991).
2. I. Yamaguchi and T. Zhang, "Phase-shifting digital holography," Opt. Lett. **22,** 1268-1270 (1997).
3. E. J. Post, "Sagnac effect," Rev. Mod.Phys. **39,** 475 (1967).
4. D. A. Jackson, A. D. Kersey and A. C. Lewin, "Fiber gyroscope with passive quadrature detection," Electron. Lett. **20,** 399-401 (1984).
5. S. K. Sheem, "Fiberoptic gyroscope with 3x3 directional coupler," Appl. Phys. Lett. **37,** 869-871 (1980).
6. Z. Yaqoob, J. G. Wu, X. Q. Cui, X. Heng and C. H. Yang, "Harmonically-related diffraction gratings-based interferometer for quadrature phase measurements," Opt. Express **14,** 8127-8137 (2006).
7. J. G. Wu, Z. Yaqoob, X. Heng, L. M. Lee, X. Q. Cui and C. H. Yang, "Full field phase imaging using a harmonically matched diffraction grating pair based homodyne quadrature interferometer," Appl. Phys. Lett. **90,** (2007).
8. M. A. Choma, C. H. Yang and J. A. Izatt, "Instantaneous quadrature low-coherence interferometry with 3x3 fiber-optic couplers," Opt. Lett. **28,** 2162-2164 (2003).
9. Z. Yaqoob, J. Fingler, X. Heng and C. Yang, "Homodyne *en face* optical coherence tomography," Opt. Lett. **31,** 1815-1817 (2006).
10. A. W. Snyder, "Coupled-mode theory for optical fibers," J. Opt. Soc. Am. **62,** 1267-1277 (1972).
11. S. K. Sheem, "Optical fiber interferometers with 3x3 directional couplers - analysis," J. Appl. Phys. **52,** 3865-3872 (1981).
12. M. V. Sarunic, M. A. Choma, C. H. Yang and J. A. Izatt, "Instantaneous complex conjugate resolved spectral domain and swept-source OCT using 3x3 fiber couplers," Opt. Express **13,** 957-967 (2005).
13. M. V. Sarunic, B. E. Applegate and J. A. Izatt, "Real-time quadrature projection complex conjugate resolved Fourier domain optical coherence tomography," Opt. Lett. **31,** 2426-2428 (2006).
14. J. R. Barry and E. A. Lee, "Performance of coherent optical receivers," Proc. IEEE **78,** 1369-1394 (1990).
15. L. G. Kazovsky, "Optical heterodyning versus optical homodyning: A comparison," J. Opt. Commun. **6,** 18-24 (1985).
16. S. D. Personic, "Image band interpretation of optical heterodyne noise," AT&T Tech. J. **50,** 213-& (1971).

#84280 - $15.00 USD Received 19 Jun 2007; revised 20 Jul 2007; accepted 24 Jul 2007; published 26 Jul 2007

17. E. J. McDowell, X. Cui, Y. Yaqoob and C. Yang, "A generalized noise variance analysis model and its application to the characterization of 1/f noise in homodyne interferometry," Opt. Express 15, 3833-3848.
18. M. E. Smith and J. H. Strange, "NMR techniques in materials physics: A review," Meas. Sci. Technol. **7,** 449-475 (1996).
19. A. H. Andersen and J. E. Kirsch, "Analysis of noise in phase contrast MR imaging," Med. Phys **23,** 857-869 (1996).
20. C. D. Constantinides, E. Atalar and E. R. McVeigh, "Signal-to-noise measurements in magnitude images from NMR phased array," Mag. Res. Med. **38,** 852-857 (1997).
21. D. Erdogmus, R. Yan, E. G. Larsson, J. C. Principe and J. R. Fitzsimmons, "Image construction methods for phased array magnetic resonance imaging," J. Magn. Reson. Imaging **20,** 306-314 (2004).
22. N. Aydin and H. S. Markus, "Time-scale analysis of quadrature Doppler ultrasound signals," IEE P-Sci. Meas. Tech. **148,** 15-22 (2001).

1. Introduction

There are a number of signal acquisition scenarios that involve the measurement of phase separated components, such as quadrature components, that are later recombined in an appropriate manner to extract phase and amplitude information. There are several reported methods by which this extraction can be performed. Interestingly, the choice of signal reconstruction algorithm can have a dramatic impact on the signal-to-noise ratio (SNR) of the resulting image or signal.

Experimental designs in which phase separated components are detected include phase shifting interferometry, optical gyroscopes, harmonic gratings-based free space quadrature interferometers, and 3x3 fiber coupler-based homodyne interferometers. Phase shifting interferometric techniques introduce small phase delays in the form of subwavelength optical path length changes [1, 2]. These phase shifted signals can then be used to retrieve phase and amplitude information. In an optical gyroscope, light beams traveling in opposite directions around a rotating path experience slightly different path lengths due to the Sagnac effect [3]. The intensity and phase retrieved from the resulting phase shifted signals can be used to determine the rotation rate [4, 5]. Harmonically related gratings pairs have recently been demonstrated to be useful in full field quadrature interferometry [6, 7]. In such setups, the interference patterns between various diffraction orders of the two gratings are acquired at multiple detectors. The harmonic relationship between the gratings results in phase separation between the detected signals that is non-trivial. The sensitivity of each of these techniques can benefit by recombining the phase separated components in such a way that the total noise is minimized.

In the case of a 3x3 fiber coupler-based system, the intrinsic, nominally 120°, phase shifts between ports of the fiber coupler can be used to decouple phase and amplitude information [8, 9]. These phase shifts arise due to evanescent coupling between fiber waveguides as described by coupled mode theory [10, 11], or more simply for 2x2 and 3x3 fiber couplers through conservation of energy [8]. 3x3 fiber coupler-based systems have been employed to construct homodyne *en face* OCT images of biological samples [9] and to remove the complex conjugate ambiguity in swept source OCT images of the ocular anterior segment [12, 13]. The simplicity of homodyne systems compared to their heterodyne counterparts is a significant implementation advantage. In addition, a properly performed homodyne experiment can provide a 3 dB improvement in SNR compared to heterodyne techniques [14-16]. It has also been demonstrated that, by using appropriate detection parameters, 1/f noise does not degrade the sensitivity of homodyne systems [17].

Quadrature components are also commonly detected in signal acquisition schemes for other biomedical imaging techniques, such as nuclear magnetic resonance (NMR), magnetic resonance imaging (MRI), and Doppler ultrasound. Like the abovementioned optical techniques, these signals must be also recombined in order to retrieve amplitude and phase information. NMR spectrometers commonly utilize two detectors, acquiring 90° phase shifted signals to allow for improved pulse power efficiency and SNR [18]. Likewise, phase shifted signals from multiple coils in MR imaging systems are combined for phase or amplitude imaging. The MR community is well aware that the SNR of the resulting images is affected

#84280 - $15.00 USD Received 19 Jun 2007; revised 20 Jul 2007; accepted 24 Jul 2007; published 26 Jul 2007

by the way the image is reconstructed [19-21]. Finally, in Doppler ultrasound systems the real and imaginary parts of the Doppler shift signals are detected in order to determine amplitude and phase, which is necessary to determine Doppler information [22].

In this manuscript we will report on the SNR advantage that can be achieved by recombining phase separated signals in an optimal manner. Our goal in each of the reported signal reconstruction algorithms is to determine the amplitude of the signal as accurately as possible. In the process we may or may not determine the phase of the signal as well. That said, we find that methods that make use of the phase information contained in the measurements perform better than those that do not. In Section 1 we will describe our 3x3 fiber coupler-based homodyne OCT system. We will then describe five different image reconstruction algorithms in Section 2, including two phase dependent methods. We theoretically determine that these algorithms achieve improved SNR as compared to the other three reconstruction methods, and find that they are capable of achieving comparable SNR to commonly employed heterodyne techniques. Notably, these algorithms are not specific to our 3x3 fiber coupler-based OCT system, but are general techniques applicable for use in signal extraction processing wherever phase separated components are available. In Section 3 we will describe our experimental setup. In Section 4 we compare our experimentally determined SNR values to those derived in Section 2, and discuss the influence of the five methods on reconstructed biological images. Finally, we state our conclusions in Section 5.

2. 3x3 homodyne OCT theory

We will first describe the 3x3 homodyne OCT system for high resolution *en face* imaging of biological samples (following Ref. 1). This scheme has the ability to decouple amplitude and phase information without the need for complex rapid scanning optical delay mechanisms

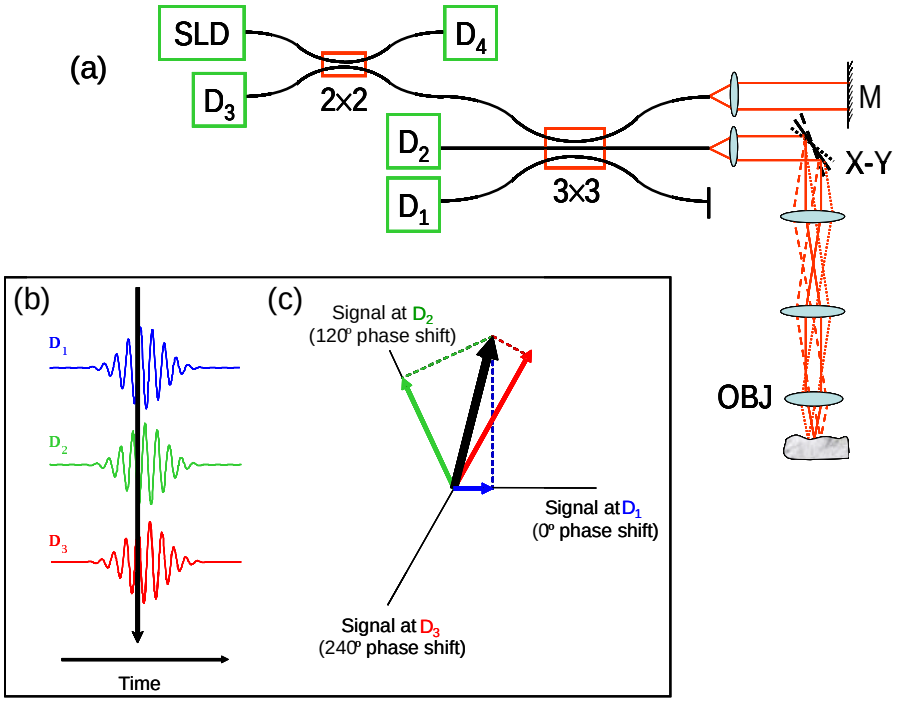

Fig. 1. (a) Experimental setup for 3x3 fiber coupler based homodyne optical coherence tomography. SLD: superluminescent diode, D_n: nth photodetector, M: mirror, X-Y: x-y scanner, OBJ: 20x microscope objective. (b) In this homodyne system the reference mirror (M) is stationary. We can think of the measured signal as a single point (black arrow) on the modulated coherence function that would be obtained if the reference arm was swept. (c) These points are the projections of a complex value onto axes separated by 120°.

#84280 - $15.00 USD Received 19 Jun 2007; revised 20 Jul 2007; accepted 24 Jul 2007; published 26 Jul 2007

used in heterodyne systems, or expensive components such as spectrometers or swept laser sources. Figure 1(a) shows the experimental setup utilized in this study. Broadband light from an SLD (λ_0=1300nm, $\Delta\lambda$=85nm) enters a 2x2 fiber coupler, followed by a 3x3 fiber coupler. Backscattered light from the sample is mixed with reference light to create an interference pattern at detectors 1-3. Detector 4 is used to monitor and correct for source fluctuations. Figure 1(b,c) diagrams the type of data that we are collecting. Using a stationary reference arm, we are essentially measuring a single point on the interferogram (represented by the thick black arrow, Fig. 1(b)). Thus, we measure three interferometric signals that can be thought of as the projections of a complex signal onto axes separated by 120° (Fig. 1(c)). The optical signal at the j[th] detector is given by:

$$P_j(z) = P_{r,j} + P_{s,j} + 2\left(1/s_j\right)\sqrt{\alpha_{41}\alpha_{4j}\alpha_{51}\alpha_{5j}P_r}\left(\sqrt{P_S(z)} \otimes \gamma(z)\right)\cos\left(\theta(z) + \varphi_j\right). \quad (1)$$

where $P_{r,j}$ and $P_{s,j}$ represent the total DC power returning from the reference and sample arms, respectively; $1/s_j$ is a scaling factor that accounts for both coupler and detector loss; P_r is the returning reference power; $P_s(z)$ is the returning coherent light from a depth z within the sample; $\gamma(z)$ is the source autocorrelation function; $\theta(z) = 2k_0z + \psi(z)$, is the phase associated with each depth in the sample, where k_0 is the optical wavenumber corresponding to the center wavelength of the source and $\psi(z)$ is the intrinsic reflection phase shift of the sample at depth z; Finally, φ_j represents the phase shifts between each of the three detectors, attributable to the intrinsic phase shifts of the 3x3 fiber coupler. The signal of interest, which describes the reflectivity profile of the sample, is the coefficient of the cosine term, which can be isolated in several ways following removal of the DC terms. Below we describe several techniques to reconstruct the coefficient of the cosine term.

3. Theoretical SNR corresponding to image reconstruction algorithms

In the following analysis we will determine the theoretical SNR for five different image reconstruction algorithms. For comparison, we will also derive the SNR corresponding to both optimal and commonly employed homodyne and heterodyne techniques. In each of the following derivations we will make the assumption that the signal at each detection port in terms of number of detected photons, is given by:

$$S_i = \tfrac{2}{n}\sqrt{P_R P_S}\,\frac{\varepsilon\tau}{h\nu}\cos\left(\theta + \varphi_i\right) \pm N_i, \quad (2)$$

where P_R and P_S are the power returning from the reference and sample arms, respectively, n is the number of detection ports ($n \geq 2$), ε is the detector quantum efficiency, τ is the integration time, h is Planck's constant, and υ is the optical frequency. N_i represents a fluctuating noise term that is zero mean, and assumed to be Gaussian distributed with standard deviation as expected given shot noise limited detection:

$$\sigma_{N_i} = \sqrt{\frac{P_r\varepsilon\tau}{nh\upsilon}} \quad (3)$$

Finally, we assume that the optical power returning from the reference arm is much greater than that returning from the sample arm ($P_R >> P_S$), which is typical when imaging highly scattering biological samples. In Eq. 2 we have assumed that the terms $P_{r,j}$ and $P_{s,j}$ from Eq. 1 have been subtracted. This can be accomplished in a practical setting by alternately blocking the sample and reference arms to measure their individual contributions.

In each of these reconstruction methods we wish to isolate a signal that is proportional to the power returning from the sample, P_S. Thus, our goal is to isolate the square of the coefficient of the cosine term in Eq. 2. In addition to this signal, we will also determine how the reconstruction method affects both the expected value and standard deviation of the fluctuating noise. These noise parameters are important factors in image quality. The standard

#84280 - $15.00 USD Received 19 Jun 2007; revised 20 Jul 2007; accepted 24 Jul 2007; published 26 Jul 2007

deviation of the noise is related to the SNR, which determines the lowest amplitude features that are visible in the image. The expected, or mean, value of the noise can add a DC shift to the image, thereby affecting the contrast of the image.

3.1 Optimal SNR in common interferometric topologies

Here we describe the theoretical SNR corresponding to common inteferometric setups. Figure 2 shows schematics of the setups that we will examine, which include 2x2 (50/50) fiber coupler-based Michelson interferometers employing a) homodyne and b) heterodyne detection. The signal and noise at each output port of the coupler can be represented by Eqs. 2 and 3 where n=2 to account for the power splitting ratios of the 50/50 fiber coupler.

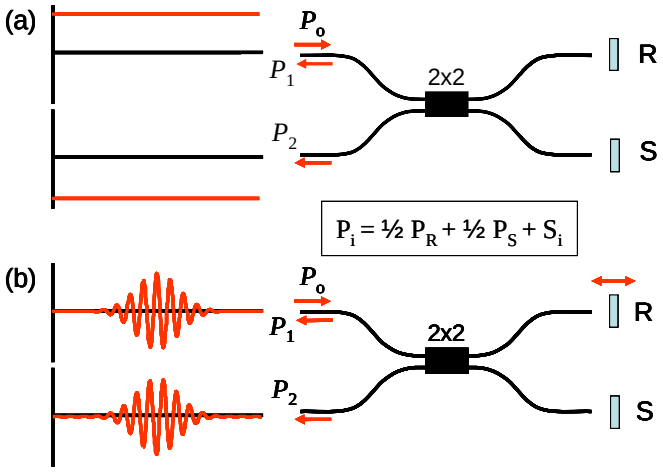

Fig. 2. 2x2 (50/50) interferometric setups utilizing a) homodyne and b) heterodyne detection. In (a) the reference mirror is stationary, while it is translated in (b). The 180° phase shifts of the fiber coupler are evident in the acquired signals at the two output ports.

The upper limit on SNR can be achieved in a homodyne experiment with perfect phase control [14-16]. In this type of experiment, the argument of the cosine in Eq. 2 can be adjusted such that the maximal signal is always detected. By subtracting the signals acquired at each port of the coupler in Fig. 2a (i.e. performing balanced detection), the ideal SNR can be determined as:

$$M_{Optimal} = \tfrac{1}{4}(S_1 - S_2)^2, \tag{4}$$

with reconstructed signal of the form:

$$Sig_{M_{Optimal}} = P_R P_S \left(\frac{\varepsilon\tau}{h\upsilon}\right)^2. \tag{5}$$

The expected value of the noise is given by:

$$E\left[M_{Optimal}(N_i)\right] = E\left[\tfrac{1}{4}(N_1 - N_2)^2\right] = \tfrac{1}{4}\left(E\left[N_1^2\right] + E\left[N_2^2\right]\right) = \tfrac{1}{2}\sigma^2. \tag{6}$$

This expression is expanded and written in terms of $E[N_i^2]$. For some of the following methods we will have terms of the form $E[N_i^4]$ as well. We can evaluate this simplified expression based on a knowledge of the variance at a single detection port: $E[N_i^2]=\sigma^2$ and $E[N_i^4]=3\sigma^4$ (where σ is given by Eq. 3). These substitutions can be made since the noise at

#84280 - $15.00 USD Received 19 Jun 2007; revised 20 Jul 2007; accepted 24 Jul 2007; published 26 Jul 2007

each port is assumed to be Gaussian. The expectation of odd powers of N_i is zero since the noise is zero mean. In a similar manner we can now evaluate the variance of this method:

$$\begin{aligned}\sigma^2_{M_{Optimal}} &= E\left[\tfrac{1}{16}\left(N_1 - N_2\right)^4\right] - \left(\tfrac{1}{2}\sigma^2\right)^2 = \\ &= \tfrac{1}{16}E\left[N_1^4\right] + \tfrac{6}{16}E\left[N_1^2\right]E\left[N_2^2\right] + \tfrac{1}{16}E\left[N_2^4\right] - \tfrac{1}{4}\sigma^4 . \\ &= \tfrac{3}{16}\sigma^4 + \tfrac{6}{16}\sigma^4 + \tfrac{3}{16}\sigma^4 - \tfrac{1}{4}\sigma^{4\,2} = \tfrac{1}{2}\sigma^4\end{aligned} \tag{7}$$

Finally, we can determine the SNR as follows:

$$SNR_{optimal} = \left(\frac{Sig_{M_{Optimal}}}{\sigma_{M_{Optimal}}}\right)\frac{P_R P_S\left(\dfrac{\varepsilon\tau}{h\upsilon}\right)^2}{\dfrac{P_R\varepsilon\tau}{\sqrt{2}2h\upsilon}} = 2\sqrt{2}\,\frac{P_S\varepsilon\tau}{h\upsilon}. \tag{8}$$

Knowledge of phase can be attained in two ways. In the first situation, the phase is known prior to the measurement. This scenario can conceivably occur in well controlled experiments where the only unknown variable is the signal amplitude. In the second situation, an estimate of the phase can be extracted from the measurement itself, and that information is then used in computing the signal amplitude. This type of phase estimation is employed in some of the following signal reconstruction algorithms. We note that the computation of signal amplitude where phase knowledge is used can be expected to be less robust and prone to systematic errors. In section 5.3, we investigate the effect of phase error on our signal reconstruction algorithms, and find that they are surprisingly robust.

Heterodyne detection is typically accomplished using an AC lock-in amplifier. The measured signal is multiplied by a sine and cosine oscillating at the signal frequency, and summed over a variable time step. The two outputs of the lock-in provide quadrature components for determination of signal amplitude and phase. The amplitude of the signal is then computed as the magnitude of the quadrature components. The signal reconstruction process can be written as the following, where S is the measured data:

$$M_{heterodyne} = \left(\sum_{i=1}^{X}\left(S_{i,1} - S_{i,2}\right)\cos\left(\Delta\omega_i\right)\right)^2 + \left(\sum_{i=1}^{X}\left(S_{i,1} - S_{i,2}\right)\sin\left(\Delta\omega_i\right)\right)^2, \tag{9}$$

The time step for each term in the summation is τ/X. In an analog mode lock-in amplifier X is effectively infinity and the summation can be replaced by an integration. As we shall see, the actual value of X (as long as it is >2) has no impact on the computed SNR. For the purpose of comparison, this method and each of the following methods leads to a reconstructed signal that is identical to Eq. 5. Derivation of the expected value and variance of the noise for this and following methods is detailed in the Appendix. The results are given by:

$$E\left[M_{heterodyne}\left(N_i\right)\right] = 2X\sigma^2 \tag{10}$$

$$\sigma^2_{heterodyne} = 4X^2\sigma^4. \tag{11}$$

which corresponds an SNR of the form:

#84280 - $15.00 USD Received 19 Jun 2007; revised 20 Jul 2007; accepted 24 Jul 2007; published 26 Jul 2007

$$SNR_{heterodyne} = \frac{P_R P_S \left(\frac{\varepsilon\tau}{h\upsilon}\right)^2}{2X\frac{P_R\varepsilon\tau}{2Xh\upsilon}} = \frac{P_S\varepsilon\tau}{h\upsilon}. \quad (12)$$

Heterodyne detection can also be improved given knowledge of the phase of the signal. In this case, the signal need only be multiplied by one phase matched sinusoidal component:

$$M_{heterodyne\ with\ phase\ knowledge} = \left(\sum_{i=1}^{X}\left(S_{i,1} - S_{i,2}\right)\cos\left(\Delta\omega_i + \theta\right)\right)^2. \quad (13)$$

The use of phase knowledge results in a decrease in noise and corresponding increase in SNR.

$$E\left[M_{heterodyne\ with\ phase\ knowledge}\right] = X\sigma^2 \quad (14)$$

$$\sigma^2_{heterodyne\ with\ phase\ knowledge} = 2X^2\sigma^4 \quad (15)$$

$$SNR_{heterodyne\ with\ phase\ knowledge} = \frac{P_R P_S \left(\frac{\varepsilon\tau}{h\upsilon}\right)^2}{\sqrt{2}X\frac{P_R\varepsilon\tau}{2Xh\upsilon}} = \sqrt{2}\frac{P_S\varepsilon\tau}{h\upsilon}. \quad (16)$$

The above expressions will be useful as benchmarks to evaluate the performance of our image reconstruction algorithms with respect to optimal SNR, as well as routinely achievable SNR performance.

3.2 Method 1

Here we begin to discuss methods for image reconstruction given phase separated components at the three ports of a 3x3 fiber coupler based OCT system. We assume ideal conditions in which the power splitting ratios for the coupler are equivalent (α_{ij}=1/3), φ_j=120°, and s_i=1, and the signal and noise at each point is given by Eqs. 2 and 3 where n=3.

The most common method to reconstruct an image is to simply square and sum the signals from each port of the fiber coupler [9]. This processing removes the cosine terms, which contribute a factor of 3/2 to the final reconstructed signal. We define method 1 as follows:

$$M_1 = \tfrac{3}{2}\left(S_1^2 + S_2^2 + S_3^2\right). \quad (17)$$

We can determine the mean value and variance of the noise to be:

$$E\left[M_1\left(N_i\right)\right] = \tfrac{9}{2}\sigma^2 \quad (18)$$

$$\sigma^2_{M_1} = \tfrac{27}{2}\sigma^4, \quad (19)$$

and find an SNR of:

#84280 - $15.00 USD Received 19 Jun 2007; revised 20 Jul 2007; accepted 24 Jul 2007; published 26 Jul 2007

$$SNR_{M_1} = \frac{P_R P_S \left(\frac{\varepsilon\tau}{h\upsilon}\right)^2}{\frac{3\sqrt{3}P_R\varepsilon\tau}{\sqrt{2}3h\upsilon}} = \frac{\sqrt{6}}{3}\frac{P_S\varepsilon\tau}{h\upsilon}. \quad (20)$$

3.3 Method 2

A second method takes advantage of instantaneous quadrature, as described by Choma *et al* [8]. Taking the signal at port 1 of the coupler, S_1, as our real signal, the imaginary signal is reconstructed as:

$$S_{IM} = \frac{S_1\cos\varphi_2 - S_2\beta}{\sin\varphi_2} \quad \beta = \sqrt{\frac{\alpha_{41}\alpha_{51}}{\alpha_{42}\alpha_{52}}}. \quad (21)$$

Using the assumptions listed above, namely φ_i=120° and α_{ij}=1/3. We are then able to reconstruct our image as the magnitude of this complex signal, (S_{RE}^2+S_{IM}^2). We can simplify the expression as follows:

$$M_2 = \tfrac{9}{4}\left(S_{RE}^2 + S_{IM}^2\right) = 3\left(S_1^2 + S_2^2 + S_1S_2\right). \quad (22)$$

We find noise parameters of the form:

$$E\left[M_2\left(N_i\right)\right] = 6\sigma^2 \quad (23)$$

$$\sigma_{M_2}^2 = 45\sigma^4, \quad (24)$$

and corresponding SNR:

$$SNR_{M_2} = \frac{P_R P_S \left(\frac{\varepsilon\tau}{h\upsilon}\right)^2}{\frac{3\sqrt{5}P_R\varepsilon\tau}{3h\upsilon}} = \frac{\sqrt{5}}{5}\frac{P_S\varepsilon\tau}{h\upsilon}. \quad (25)$$

3.4 Method 3

This method makes use of phase information during signal amplitude computations. We again follow Choma's method for obtaining instantaneous quadrature, and calculate the phase at each point in our image, θ=tan^{-1}(S_{IM}/S_{RE}). The estimated phase is then used to divide out the cosine terms present in Eq. 2. Finally, we scale and sum the three signals using scaling factors, a_i, constrained to sum to 1. In this way, we isolate the desired signal as follows:

$$M_3 = \frac{9}{4}\left[\frac{a_1S_1}{\cos\left(\theta+\varphi_1\right)} + \frac{a_2S_2}{\cos\left(\theta+\varphi_2\right)} + \frac{a_3S_3}{\cos\left(\theta+\varphi_3\right)}\right]^2. \quad (26)$$

Scaling factors, a_i, are determined by substituting the measured phases, as well as φ_i, and minimizing the resulting noise. For example, if the values of θ and φ_i for a given channel produce a cosine value close to zero, then the noise would increase greatly after dividing it by

#84280 - $15.00 USD Received 19 Jun 2007; revised 20 Jul 2007; accepted 24 Jul 2007; published 26 Jul 2007

this small number. Hence, this channel would be weighted the least compared to the others. And conversely, maximally interfering signals (large cosine value) are weighted more heavily than others. Since the noise in each channel is equivalent, larger interferometric signals should lead to an increase in SNR. The values of the scaling factors can be expressed as a function of the phase as well as the phase shifts between subsequent ports:

$$a_i = \tfrac{2}{3}\left[\cos^2\left(\theta + \varphi_i\right)\right]. \tag{27}$$

The noise parameters and SNR that correspond to this method are:

$$E\left[M_3\left[N_i\right]\right] = \tfrac{3}{2}\sigma^2 \tag{28}$$

$$\sigma^2_{M_3} = \tfrac{9}{2}\sigma^4 \tag{29}$$

$$SNR_{M_3} = \frac{P_R P_S\left(\dfrac{\varepsilon\tau}{h\upsilon}\right)^2}{\dfrac{3P_R\varepsilon\tau}{\sqrt{2}3h\upsilon}} = \sqrt{2}\,\frac{P_S\varepsilon\tau}{h\upsilon}. \tag{30}$$

This method can be generalized for an nxn fiber coupler based interferometer. In this case, the reconstruction based on Method 3 is given by:

$$\frac{n^2}{4}\left(\sum_{i=1}^{n}\frac{a_i S_i}{\cos\left(\theta + \dfrac{2\pi}{n}(i-1)\right)}\right)^2, \tag{31}$$

where a_i is:

$$a_i = \frac{2}{n}\cos^2\left(\theta + \frac{2\pi}{n}(i-1)\right). \tag{32}$$

As was previously mentioned, the sum over all *a* values is 1. The above expressions can be used to determine the expected value and variance of the noise for this generalized reconstruction method:

$$E\left[M_{3,\ n\ ports}\right] = \frac{n}{2}\sigma^2 \tag{33}$$

$$\sigma^2_{M_3,\ n\ ports} = \tfrac{1}{2}n^2\sigma^4, \tag{34}$$

With SNR determined as:

$$SNR_{M_{3,\ n\ ports}} = \frac{P_R P_S\left(\dfrac{\varepsilon\tau}{h\upsilon}\right)^2}{\dfrac{nP_R\varepsilon\tau}{\sqrt{2}nh\upsilon}} = \sqrt{2}\,\frac{P_S\varepsilon\tau}{h\upsilon}. \tag{35}$$

#84280 - $15.00 USD Received 19 Jun 2007; revised 20 Jul 2007; accepted 24 Jul 2007; published 26 Jul 2007

This is expression is the same as that given in Eq. 30. Interestingly, the SNR associated with this method is independent of the number of output ports available for signal collection.

3.5 Methods 4 and 5

Finally we wish to discuss two additional reconstruction methods that are directly analogous to the processing performed by AC lock-in detection, and most easily understood in the context of a large number of detection ports (although these techniques will work as long as n≥3). Instead of expressing our interferogram in terms of pathlength mismatch, we can write it in terms of phase delay, where each detection port samples a different phase delay. Thus by multiplying the measured signal by sines and cosines phase shifted similarly to each of the output ports, we can estimate the amplitude of the signal by averaging the result. The signal is reconstructed as:

$$M_4 = \left(\sum_{i=1}^{n} S_i \cos(\phi_i) \right)^2 + \left(\sum_{i=1}^{n} S_i \sin(\phi_i) \right)^2, \tag{36}$$

and the noise is given by:

$$E[M_4(N_i)] = n\sigma^2 \tag{37}$$

$$\sigma_{M_4}^2 = n^2\sigma^4. \tag{38}$$

We find SNR equivalent to the heterodyne case:

$$SNR_{M4} = \left(\frac{P_R P_S \left(\frac{\varepsilon\tau}{h\upsilon} \right)^2}{n \frac{P_R \varepsilon\tau}{nh\upsilon}} \right) = \frac{P_S \varepsilon\tau}{h\nu}. \tag{39}$$

Likewise, with knowledge of the phase of the signal from quadrature components in section 3.3, the signal can be reconstructed using only one sinusoidal component:

$$M_5 = \left(\sum_{i=1}^{n} S_i \cos(\phi_i + \theta) \right)^2 \tag{40}$$

$$E[M_5(N_i)] = \frac{n}{2}\sigma^2 \tag{41}$$

$$\sigma_{M_5}^2 = \tfrac{1}{2} n^2\sigma^4. \tag{42}$$

The noise is reduced by a factor of 2, giving an SNR of:

$$SNR_{M5} = \left(\frac{P_R P_S \left(\frac{\varepsilon\tau}{h\upsilon} \right)^2}{\frac{n}{\sqrt{2}} \frac{P_R \varepsilon\tau}{nh\upsilon}} \right) = \sqrt{2} \frac{P_S \varepsilon\tau}{h\nu}. \tag{43}$$

#84280 - $15.00 USD Received 19 Jun 2007; revised 20 Jul 2007; accepted 24 Jul 2007; published 26 Jul 2007

The results of these derivations can be found in Table 1. We note that the two methods that incorporate phase information, Methods 3 and 5, are predicted to have better SNR in comparison with the other methods. It is interesting to note that Methods 3 and 5 are predicted to have the same SNR. In fact, as is derived in the Appendix, a substitution of Eq. 32 for a_i converts Method 3 into a form identical to Method 5. However similar, we note that these methods differ in the case where the phase shifts at the ports of the fiber coupler are not equally spaced (i.e. $\varphi_i \neq 2\pi(i-1)/n$). In this case, the a_i's can be determined through a minimization, and the method will produce an image with a different SNR than that derived above. Method 5 requires that the phase shifts be equally spaced, and will not perform well under these conditions.

Finally, we note that although we have assumed shot noise limited detection in these derivations, the five methods will perform the same with respect to one another so long as the dominant noise source is white.

4. Experimental methods

The system depicted in Fig. 1 was calibrated to determine accurate values for φ_i and s_i. In order to make SNR measurements, a mirror was placed in the sample arm to serve as an ideal reflector, which was attenuated (-70 dB) such that sample arm shot noise was negligible compared to that from the reference arm. A beam chopper was used to alternate measurements of signal and background noise. In order to assure that we were using our homodyne system to acquire shot noise limited data, as opposed to dominant 1/f noise, we sampled quickly, at 800 kHz, and limited our data averaging time (~0.65 ms) following the results of Ref. [17]. Both signal and noise data were reconstructed using the five methods described above, and the SNR was determined as the mean signal divided by the standard deviation of the noise. The methods were also compared based on the mean value of the reconstructed noise.

We then used the 3x3 homodyne OCT system to acquire several images. Our system resolution has been measured to be approximately 14 μm in the axial direction, and 9.4 μm in the lateral direction. First, we imaged a highly attenuated Air Force test target (-50 dB) in order to visualize the relative performance of the three methods in a low signal situation. We then imaged stage 54 *Xenopus laevis* tadpoles. Each data set was processed using the five image reconstruction algorithms described above, and displayed on equivalent color scales. The improved image contrast obtained using reconstruction Methods 3 and 5 confirms our theoretical findings in biological samples.

Table 1. Comparison of theoretical and experimental results. Notably, the phase dependent methods (3 and 5) show superior SNR and noise performance with respect to the others.

Reconstruction Method	**Method 1**	**Method 2**	**Method 3**	**Method 4**	**Method 5**
Theoretical SNR	$\frac{\sqrt{6}P_S\varepsilon\tau}{3h\nu}$	$\frac{\sqrt{5}P_S\varepsilon\tau}{5h\nu}$	$\frac{\sqrt{2}P_S\varepsilon\tau}{h\nu}$	$\frac{P_S\varepsilon\tau}{h\nu}$	$\frac{\sqrt{2}P_S\varepsilon\tau}{h\nu}$
Experimental SNR (dB)	88.0	85.6	91.0	90.6	91.1
Theoretical Comparison to Method 5 (dB)	-2.4	-5	0	-1.5	0
Experimental Comparison to Method 5 (dB)	-3.1	-5.4	-0.04	-0.4	0
Theoretical Mean Noise	$\frac{9}{2}\sigma^2$	$6\sigma^2$	$\frac{3}{2}\sigma^2$	$3\sigma^2$	$\frac{3}{2}\sigma^2$
Experimental Mean Noise (10^{-6})	4.6	5.9	2.4	2.9	2.4

#84280 - $15.00 USD Received 19 Jun 2007; revised 20 Jul 2007; accepted 24 Jul 2007; published 26 Jul 2007

5. Results and discussion

5.1 Experimental SNR results

We evaluated our reconstruction methods base on data acquired with an attenuated mirror in the sample arm. Figure 3 displays a typical reconstructed trace, showing alternating signal and noise measurements as the sample beam was chopped. The SNR of the reconstructed signals were determined, as well as the mean value of the noise. Both calculations were made using the data depicted in Fig. 3. The results can be seen in Table 1, showing that Methods 3 and 5, which take advantage of the known phase in order to minimize the noise, perform significantly better than the other methods in terms of SNR. In close agreement with our theoretical predictions, we found an SNR enhancement of up to 5.4 dB over the phase independent methods. These two methods also leave the smallest remaining DC noise after signal reconstruction. However, we note that these two methods do not match theoretical predictions as closely as the other three methods. It is reassuring that Methods 3 and 5 vary from theory in a comparable manner, since they perform very similar processing; however, the exact cause of this discrepancy is unclear to the authors at this time.

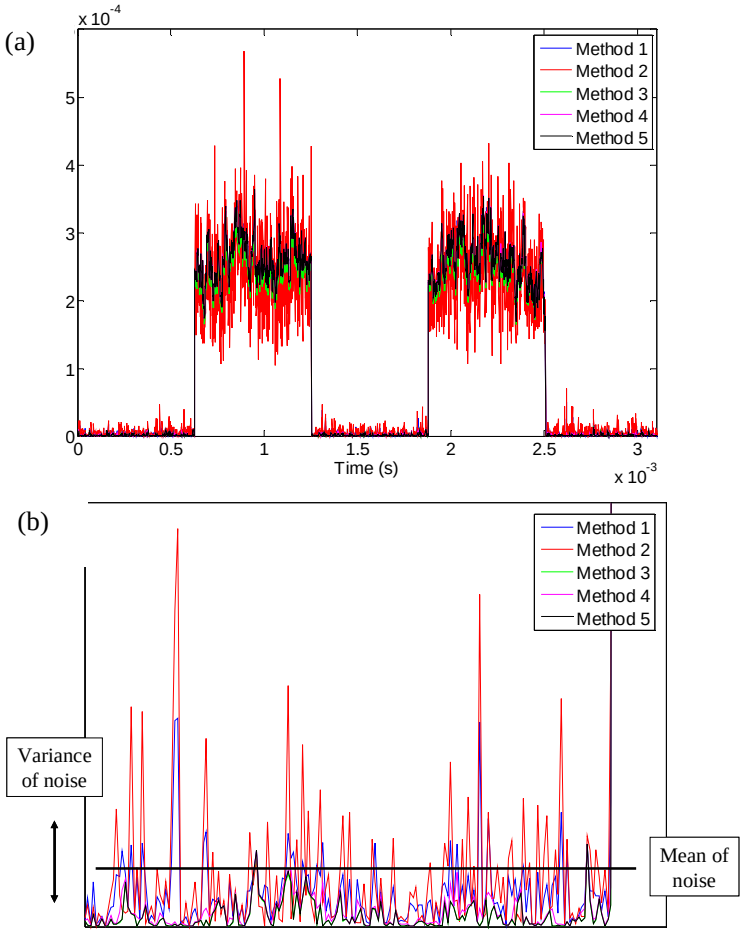

Fig. 3. (a) Reconstructed signals from an attenuated mirror. A beam chopper was used to make measurements of both signal and background noise, which were used to experimentally determine the SNR of the five methods. (b) A magnified view of the noise from (a) depicting experimentally determined values for the mean and variance of the noise.

#84280 - $15.00 USD Received 19 Jun 2007; revised 20 Jul 2007; accepted 24 Jul 2007; published 26 Jul 2007

5.2 Imaging results

The SNR improvement noted in the previous section is quite dramatic in our reconstructed images. Figure 4 shows a portion of an Air Force test target. The resolution target was highly attenuated (-50 dB) such that the optical power returning through the sample arm was very low. Each of the images shown in Fig. 4 was reconstructed from the same raw data using Methods 1-5 described above. Additionally, each image is displayed on the same color scale. We see that for the image reconstructed using Method 2 the bars on the test target can barely be discriminated from the background. The image reconstructed using Method 1 is better, but there is still relatively little contrast between the bars and the background noise. As predicted by the theoretical sensitivity analysis, Methods 3 and 5 produce images with a marked increase in contrast compared to the others. The bars of the Air Force test target are clearly distinguishable in panels (3) and (5) of Fig 5.

Our reconstruction algorithms were also tested on data from biological images. Fig. 5 (first column) shows an image of structures in the anterior, medial portion of a stage 54 *Xenopus laevis* tadpole. Again, Methods 3 and 5 produced images that more clearly

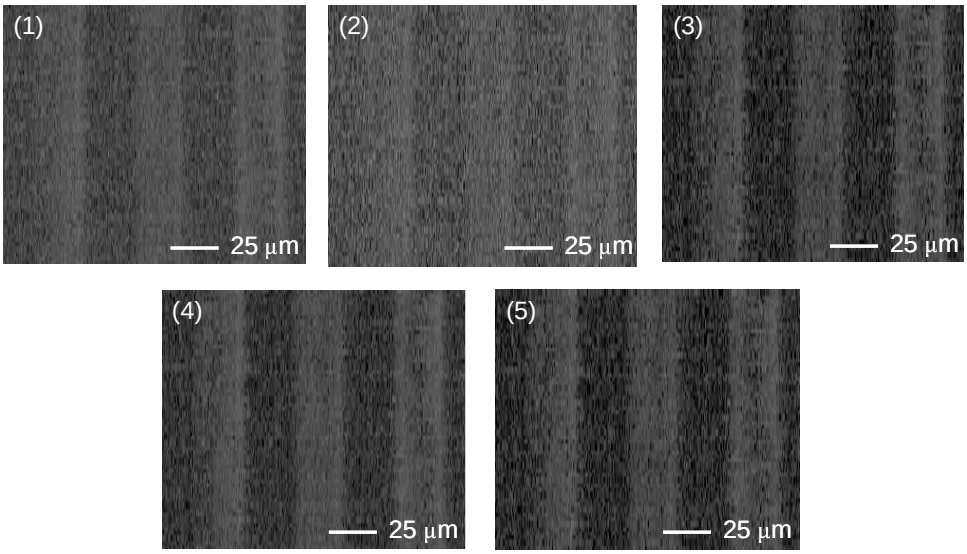

Fig. 4. These images show a portion of a highly attenuated Air Force test target, representing a very low signal situation. The three images were reconstructed from a single data set and reconstructed using Methods 1-5 (described above). Methods 3 and 5 clearly perform better than the others, showing a notable increase in contrast between the bars of the test target and the background.

distinguish biological structure from background noise. The nuclei of the cellular structures at the bottom of the image are more visible. The ability to achieve superior SNR based only on reconstruction algorithm implies that, to achieve the same SNR as through commonly used reconstruction algorithms, the optical power incident on fragile biological tissues can be reduced. In Fig. 5 (second column) we have subtracted the DC value of the noise in each image in order to compare the noise variance between images. When a portion of the background noise is magnified (Fig. 5, column 3), there is significantly more background fluctuation in images corresponding to Methods 1 and 2 than in the other images.

We have seen in the above experimental results that Methods 3 and 5 are capable of producing images with the highest SNR. In these methods, knowledge of the phase at each point in the image was used to minimize the noise at that point. In essence, these algorithms utilize more of the available information than the other methods.

#84280 - $15.00 USD Received 19 Jun 2007; revised 20 Jul 2007; accepted 24 Jul 2007; published 26 Jul 2007

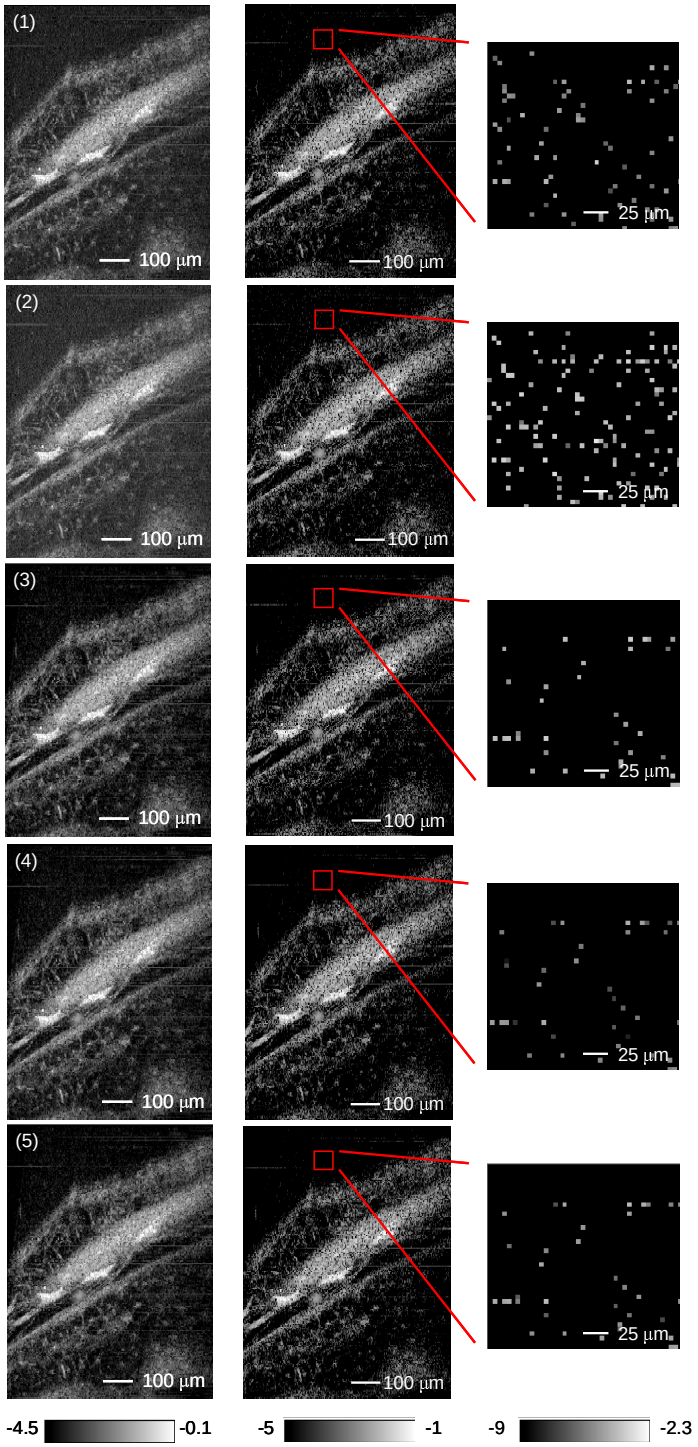

Fig. 5. In the first column the image reconstruction algorithms were evaluated on images from a stage 54 Xenopus tadpole. Again, Methods 3 and 5 produced images with improved SNR, more clearly distinguishing biological features such as cell nuclei from background noise. In the second column of images the DC noise has been subtracted from the image. The increase noise variance is now visible in the background of the images corresponding to Methods 1 and 2 in a blown up portion of the background (third column)

#84280 - $15.00 USD Received 19 Jun 2007; revised 20 Jul 2007; accepted 24 Jul 2007; published 26 Jul 2007

5.3 Robustness to phase error

The performance of each of the signal reconstruction methods depends on appropriate calibration of the 3x3 homodyne OCT system. However, Methods 3 and 5 are strongly dependent on correct calculation of the phase. Determination of the phase depends on exact knowledge of the loss scaling coefficients, s_i, and the angles between adjacent ports of the fiber coupler, φ_{ij}. Uncertainty in these values leads to uncertainly in the phase at various points in the image, and additionally leads to an improper choice of noise minimization coefficients, a_i, in Method 3. To reduce the effects of this potential problem, we calibrated the 3x3 system immediately before image acquisition, making the assumption that drifts in the system calibration parameters are slow.

Additionally, we investigated the impact of phase error on the SNR of the reconstruction methods. To do this, we computed the SNR corresponding to each method using a phase $\Theta+d\theta$, where $d\theta$ is a phase error that varies from 0 through $\pi/2$. The results are plotted in Fig. 6 in terms of the SNR coefficient (i.e. the coefficient of $P_S\varepsilon\tau/h\upsilon$). The computation shows that Method 3 and 5 are surprisingly robust in the presence of phase error. Very large phase errors may be incorporated before these methods drop below the others in terms of SNR. These results imply that the phase-dependent methods not only provide improved SNR, but are relatively insensitive to errors in system calibration.

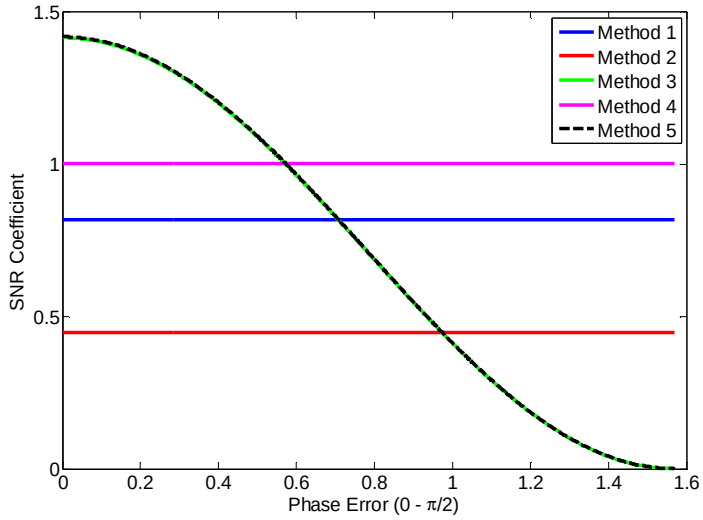

Fig. 6. SNR is plotted verses phase error for the five reconstruction methods. Only Methods 3 and 5 are phase dependent. Here, we see that these methods are relatively robust to phase error, only dropping below the other methods for fairly large errors in phase.

6. Conclusions

In conclusion, we have demonstrated the effect of image reconstruction algorithm on the SNR when phase separated components are detected. We compared five potential methods for reconstructing an image from the three outputs of a 3x3 fiber coupler-based homodyne OCT system, and demonstrated that algorithms which use knowledge of the phase at each point in the image to minimize noise perform significantly better than the others in terms of SNR. This holds true for both homodyne and heterodyne techniques. The algorithms showed an SNR increase of up to 5 dB over the other methods, and were found to perform better than the most commonly used form of heterodyne detection. This increase in SNR was evident in improved contrast, as well as overall image quality, in images from both an Air Force test target as well as biological samples. Additionally, we found that these phase-dependent methods are relatively robust in terms of phase error. Finally, we note that our analysis is not

#84280 - $15.00 USD Received 19 Jun 2007; revised 20 Jul 2007; accepted 24 Jul 2007; published 26 Jul 2007

restricted to 3x3 homodyne OCT, but can be applied to any situation in which phase separated components are combined to decouple phase and amplitude information.

Acknowledgements

This work was supported by a NSF Career Award, BES-0547657. E.J. McDowell acknowledges support from an NIH Ruth L. Kirschtein NRSA fellowship, EB006694.

Appendix

A.1 Derivation of variance for heterodyne detection

$$E\left[M_{heterodyne}(N_i)\right] = E\left[\begin{array}{l}\left(\sum_{i=1}^{X}\left(N_{i,1}-N_{i,2}\right)\cos\left(\Delta\omega_i\right)\right)^2 \\ +\left(\sum_{i=1}^{X}\left(N_{i,1}-N_{i,2}\right)\sin\left(\Delta\omega_i\right)\right)^2\end{array}\right]$$

$$= E\left[\sum_{i=1}^{X}\left(N_{i,1}^2+N_{i,2}^2\right)\left(\cos^2\left(\Delta\omega_i\right)+\sin^2\left(\Delta\omega_i\right)\right)\right] = 2XE\left[N_i^2\right] = 2X\sigma^2$$

$$E\left[M_{heterodyne}(N_i)^2\right] = E\left[\left(\begin{array}{l}\left(\sum_{i=1}^{X}\left(N_{i,1}-N_{i,2}\right)\cos\left(\Delta\omega_i\right)\right)^2 \\ +\left(\sum_{i=1}^{X}\left(N_{i,1}-N_{i,2}\right)\sin\left(\Delta\omega_i\right)\right)^2\end{array}\right)^2\right].$$

$$= E\left[\begin{array}{l}\sum_{i=1}^{X}\left(N_{i,1}-N_{i,2}\right)^4\cos^4\left(\Delta\omega_i\right) \\ +3\sum_{i=1}^{X}\sum_{\substack{j=1\\ i\neq j}}^{X}\left(N_{i,1}-N_{i,2}\right)^2\cos^2\left(\Delta\omega_i\right)\left(N_{j,1}-N_{j,2}\right)^2\cos^2\left(\Delta\omega_j\right) \\ +\sum_{i=1}^{X}\left(N_{i,1}-N_{i,2}\right)^4\sin^4\left(\Delta\omega_i\right) \\ +3\sum_{i=1}^{X}\sum_{\substack{j=1\\ i\neq j}}^{X}\left(N_{i,1}-N_{i,2}\right)^2\sin^2\left(\Delta\omega_i\right)\left(N_{j,1}-N_{j,2}\right)^2\sin^2\left(\Delta\omega_j\right) \\ +2\sum_{i}^{X}\left(N_{i,1}-N_{i,2}\right)^4\cos^2\left(kv\tau_i\right)\sin^2\left(\Delta\omega_i\right) \\ +2\sum_{i=1}^{X}\sum_{\substack{j=1\\ i\neq j}}^{X}\left(N_{i,1}-N_{i,2}\right)^2\cos^2\left(\Delta\omega_i\right)\left(N_{j,1}-N_{j,2}\right)^2\sin^2\left(\Delta\omega_j\right) \\ +4\sum_{i=1}^{X}\sum_{\substack{j=1\\ i\neq j}}^{X}\left(N_{i,1}-N_{i,2}\right)^2\cos\left(\Delta\omega_i\right)\sin\left(\Delta\omega_i\right)\left(N_{j,1}-N_{j,2}\right)^2\cos\left(\Delta\omega_j\right)\sin\left(\Delta\omega_j\right)\end{array}\right]$$

#84280 - $15.00 USD Received 19 Jun 2007; revised 20 Jul 2007; accepted 24 Jul 2007; published 26 Jul 2007

where $E[(N_{i,1}-N_{i,2})^4]=12\sigma^4$ and $E[(N_{i,1}-N_{i,2})^2]=4\sigma^4$.

$$
\begin{aligned}
&= 12\sigma^4 \sum_{i=1}^{X}\sum_{j=1}^{X} \cos^2(\Delta\omega_i)\cos^2(\Delta\omega_j) \\
&\quad + 12\sigma^4 \sum_{i=1}^{X}\sum_{j=1}^{X} \sin^2(\Delta\omega_i)\sin^2(\Delta\omega_j) \\
&\quad + 8\sigma^4 \sum_{i=1}^{X}\sum_{j=1}^{X} \cos^2(\Delta\omega_i)\sin^2(\Delta\omega_j) \\
&\quad + 16\sigma^4 \sum_{i=1}^{X}\sum_{j=1}^{X} \cos(\Delta\omega_i)\sin(\Delta\omega_i)\cos(\Delta\omega_j)\sin(\Delta\omega_j)
\end{aligned}
$$

$$= 12\sigma^4 \frac{X^2}{4} + 12\sigma^4 \frac{X^2}{4} + 8\sigma^4 \frac{X^2}{4} = 8\sigma^4 X^2$$

$$\sigma^2_{heterodyne} = 8\sigma^4 X^2 - \left(2X\sigma^2\right)^2 = 4X^2\sigma^4$$

A.2 Derivation of variance for heterodyne detection with phase knowledge

$$E\left[M_{heterodyne\ \ with\ \ phase\ \ knowledge}(N_i)\right] = E\left[\left(\sum_{i=1}^{X}\left(N_{i,1}-N_{i,2}\right)\cos(\Delta\omega_i)\right)^2\right]$$

$$= E\left[\sum_{i=1}^{X}\left(N_{i,1}^2+N_{i,2}^2\right)\cos^2(\Delta\omega_i)\right] = E\left[\left(N_{i,1}^2+N_{i,2}^2\right)\right]\frac{X}{2} = 2\sigma^2\frac{X}{2} = X\sigma^2$$

$$E\left[M_{heterodyne\ \ with\ \ phase\ \ knowledge}(N_i)^2\right] = E\left[\left(\sum_{i=1}^{X}\left(N_{i,1}-N_{i,2}\right)\cos(\Delta\omega_i)\right)^4\right]$$

$$
= E\left[\begin{array}{l}
\displaystyle\sum_{i=1}^{X}\left(N_{i,1}-N_{i,2}\right)^4\cos^4(\Delta\omega_i) \\
\displaystyle +3\sum_{i=1}^{X}\sum_{\substack{j=1\\ i\neq j}}^{X}\left(N_{i,1}-N_{i,2}\right)^2\cos^2(\Delta\omega_i)\left(N_{j,1}-N_{j,2}\right)^2\cos^2(\Delta\omega_j)
\end{array}\right]
$$

$$= 12\sigma^4 \sum_{i=1}^{X}\sum_{j=1}^{X} \cos^2(\Delta\omega_i)\cos^2(\Delta\omega_j) = 12\sigma^4 \sum_{i=1}^{X}\cos^2(\Delta\omega_i)\sum_{j=1}^{X}\cos^2(\Delta\omega_j)$$

$$= 12\sigma^4 \frac{X^2}{4} = 3\sigma^4 X^2$$

#84280 - $15.00 USD Received 19 Jun 2007; revised 20 Jul 2007; accepted 24 Jul 2007; published 26 Jul 2007

$$\sigma^2_{heterodyne\ \ with\ \ phase\ \ knowledge} = 3\sigma^4 X^2 - \left(X\sigma^2\right)^2 = 2X^2\sigma^4$$

A.3 Derivation of variance for Method 1

$$E\left[M_1(N_i)\right] = E\left[\tfrac{3}{2}\left(N_1^2 + N_2^2 + N_3^2\right)\right] = \tfrac{9}{2}E\left[N_i^2\right] = \tfrac{9}{2}\sigma^2$$

$$E\left[M_1(N_i)^2\right] = E\left[\tfrac{9}{4}\left(N_1^2 + N_2^2 + N_3^2\right)^2\right]$$

$$= E\left[\tfrac{9}{4}\left(N_1^4 + N_2^4 + N_3^4 + 2N_1^2N_2^2 + 2N_1^2N_3^2 + 2N_2^2N_3^2\right)\right]$$

where $E[(N_i)^4]=3\sigma^4$ and $E[(N_i)^2]=\sigma^2$.

$$= \tfrac{9}{4}\left(3E\left[N_i^4\right] + 6E\left[N_i^2\right]E\left[N_i^2\right]\right) = \tfrac{81}{4}\sigma^4 + \tfrac{54}{4}\sigma^4 = \tfrac{135}{4}\sigma^4$$

$$\sigma^2_{M_1} = \tfrac{135}{4}\sigma^4 - \tfrac{81}{4}\sigma^4 = \tfrac{27}{2}\sigma^4$$

A.4 Derivation of variance for Method 2

$$E\left[M_2(N_i)\right] = E\left[3\left(N_1^2 + N_2^2 + N_1N_2\right)\right] = 3\left(2E\left[N_i^2\right]\right) = 6\sigma^2$$

$$E\left[M_2(N_i)^2\right] = E\left[9\left(N_1^2 + N_2^2 + N_1N_2\right)^2\right]$$

$$= E\left[9\left(N_1^4 + N_2^4 + 3N_1^2N_2^2 + 2N_1^3N_2 + 2N_1N_2^3\right)\right]$$

$$= 9\left(2E\left[N_i^4\right] + 3E\left[N_i^2\right]E\left[N_i^2\right]\right) = 54\sigma^4 + 27\sigma^4 = 81\sigma^4$$

$$\sigma^2_{M_2} = 81\sigma^4 - \left(6\sigma^2\right)^2 = 45\sigma^4$$

A.5 Derivation of variance for Method 3

In order to derive the variance for Method 3 we will, for simplicity, choose $\theta=0$ (although any value of θ will give an equivalent solution), setting $a_1=2/3$, $a_2=1/6$, $a_3=1/6$.

#84280 - $15.00 USD Received 19 Jun 2007; revised 20 Jul 2007; accepted 24 Jul 2007; published 26 Jul 2007

$$E[M_3(N_i)] = E\left[\tfrac{9}{4}\left(\frac{\tfrac{2}{3}N_1}{1} + \frac{\tfrac{1}{6}N_2}{-\tfrac{1}{2}} + \frac{\tfrac{1}{6}N_3}{-\tfrac{1}{2}}\right)^2\right] = E\left[\tfrac{9}{4}\left(\tfrac{2}{3}N_1 - \tfrac{1}{3}N_2 - \tfrac{1}{3}N_3\right)^2\right]$$

$$= \tfrac{9}{4}\left(\tfrac{4}{9}E[N_1^2] + \tfrac{1}{9}E[N_2^2] + \tfrac{1}{9}E[N_3^2]\right) = \sigma^2 + \tfrac{1}{4}\sigma^2 + \tfrac{1}{4}\sigma^2 = \tfrac{3}{2}\sigma^2$$

$$E[M_3(N_i)^2] = E\left[\tfrac{81}{16}\left(\tfrac{4}{9}N_1^2 - \tfrac{4}{9}N_1N_2 - \tfrac{4}{9}N_1N_3 + \tfrac{2}{9}N_2N_3 + \tfrac{1}{9}N_2^2 + \tfrac{1}{9}N_3^2\right)^2\right]$$

$$= \frac{81}{16}\left(\tfrac{18}{81}3\sigma^4 + \tfrac{54}{81}\sigma^4\right) = \frac{27}{4}\sigma^4$$

$$\sigma_{M_3}^2 = \tfrac{27}{4}\sigma^4 - \tfrac{9}{4}\sigma^4 = \tfrac{9}{2}\sigma^4$$

A.6 Derivation of variance for Method 3, n ports

$$E[M_{3,\ n\ ports}(N_i)] = E\left[\frac{n^2}{4}\left(\sum_{i=1}^{n}\frac{a_iN_i}{\cos\left(\theta + \frac{2\pi}{n}(i-1)\right)}\right)^2\right]$$

$$= E\left[\frac{n^2}{4}\sum_{i=1}^{n}\frac{a_i^2N_i^2}{\cos^2\left(\theta + \frac{2\pi}{n}(i-1)\right)}\right] = \frac{n^2}{4}E[N_i^2]\sum_{i=1}^{n}\tfrac{4}{n^2}\cos^2\left(\theta + \frac{2\pi}{n}(i-1)\right)$$

$$= \frac{n}{2}E[N_i^2] = \frac{n}{2}\sigma^2$$

$$E[M_{3,\ n\ ports}(N_i)^2] = E\left[\frac{n^4}{16}\left(\sum_{i=1}^{n}\frac{a_iN_i}{\cos\left(\theta + \frac{2\pi}{n}(i-1)\right)}\right)^4\right]$$

$$= E\left[\frac{n^4 2^4}{16n^4}\left(\sum_{i=1}^{n}\cos\left(\theta + \frac{2\pi}{n}(i-1)\right)N_i\right)^4\right]$$

#84280 - $15.00 USD Received 19 Jun 2007; revised 20 Jul 2007; accepted 24 Jul 2007; published 26 Jul 2007

This equation is of the same form as the heterodyne detection method described in section A.2, and can be solved in a similar manner

A.7 Derivation of variance for Methods 4 and 5

Beginning with the reconstruction methods defined in Eqs. 36 and 40, as well as the signal and noise at each port given by Eqs. 2 and 3 where n=3, the expected value and variance of the noise for these methods can be determined following the analysis in section A.1 and A.2.

#84280 - $15.00 USD Received 19 Jun 2007; revised 20 Jul 2007; accepted 24 Jul 2007; published 26 Jul 2007